Automated Processing of Sea Surface Images for the Determination of Whitecap Coverage

27 November 2024 14:51

Callaghan 2009

Automated Processing of Sea Surface Images for the Determination of Whitecap Coverage

ADRIAN H. CALLAGHAN AND MARTIN WHITE

Department of Earth and Ocean Sciences, National University of Ireland, Galway, Galway, Ireland

(Manuscript received 27 February 2008, in final form 15 July 2008)

ABSTRACT

Sea surface images have been collected to determine the percentage whitecap coverage (W) since the late 1960s. Image processing methods have changed dramatically since the beginning of whitecap studies. An automated whitecap extraction (AWE) technique has been developed at the National University of Ireland, Galway, that allows images to be analyzed for percentage whitecap coverage without the need of a human analyst. AWE analyzes digital images and determines a suitable threshold with which whitecaps can be separated from unbroken background water. By determining a threshold for each individual image, AWE is suitable for images obtained in conditions of changing ambient illumination. AWE is also suitable to process images that have been taken from both stable and nonstable platforms (such as towers and research vessels, respectively). Using techniques based on derivative analysis, AWE provides an objective method to determine an appropriate threshold for the identification of whitecaps in sea surface images without the need for a human analyst. The automated method allows large numbers of images to be analyzed in a relatively short amount of time. AWE can be used to analyze hundreds of images per individual W data point, which produces more convergent values of W.

1. Introduction

Breaking waves trap and entrain air into the water column, forming a rising bubble plume that manifests itself as a whitecap on the sea surface. Because of their mechanism of formation and composition and their distinctive white color, whitecaps are an important oceanographic feature.

Actively breaking waves allow the transfer of momentum from waves to the surface water currents. Whitecaps formed from actively breaking waves are a visual representation of wave energy dissipation, and previous studies have striven to use the surface coverage of these whitecaps as a means of quantifying energy dissipation from breaking waves (e.g., Kraan et al. 1996 and Guan et al. 2007). Whitecaps are an important mechanism for the air–sea exchange of gases such as CO_2. Laboratory experiments (e.g., Asher et al. 1996) have shown a direct relationship between the areal coverage of simulated breaking waves and the gas transfer coefficients of a range of gases, including CO_2. Bubble bursting processes within whitecaps produce primary marine aerosols that contribute to climate regulation (O'Dowd and de Leeuw 2007). Because of their color, whitecaps are effective reflectors of incoming solar radiation. Frouin et al. (2001) estimated that whitecaps exert a negative global average radiative forcing of approximately 0.03 W m^{-2}. Gordon (1997) stated that an atmospheric correction term is needed for the removal of the effect of whitecaps in the determination of ocean color from satellites. Whitecaps increase the microwave emissivity of the sea surface, which affects the retrieval of the surface wind vector from ocean microwave radiometer measurements (Wentz 1992).

A common way to quantify whitecaps is to measure the percentage area of the sea surface covered by whitecaps from sea surface images. The percentage of the sea surface covered by whitecaps is denoted W. Measured values of W are typically related to environmental parameters such as wind speed, wind friction velocity, wave field characteristics, and water temperature to provide model estimates of W. These models of W can subsequently be used as inputs to other models, such as those for primary marine aerosol production. For example, the whitecap method can be used to estimate the interfacial flux of the primary marine aerosol from the sea surface by combining an empirically derived model of whitecap coverage and laboratory-based

Corresponding author address: Adrian Callaghan, Department of Earth and Ocean Sciences, MRI Building, National University of Ireland, Galway, Galway, Republic of Ireland.
E-mail: callaghan.adrian@gmail.com

DOI: 10.1175/2008JTECHO634.1

W: percentage of sea surface covered by whitecaps

measurements of primary marine aerosol production from simulated whitecaps (Lewis and Schwartz 2004).

Many different methods have been employed by various authors to retrieve W from sea surface images, and these methods have changed through time to reflect advances in photographic and computing hardware. The majority of these studies have involved the need of a human analyst to manually determine a suitable criterion to distinguish between whitecaps and unbroken background water in sea surface images. This criterion was then applied to individual images or groups of images to determine W. The use of manual methods to determine W from images can be very time consuming and highly subjective. Two previous studies (Lafon et al. 2004, 2007, hereafter LP04 and LP07, respectively) have used an automated whitecap detection algorithm to process sea surface images for W. The image processing technique was developed at the Laboratoire d'Etude des Echanges Particulaires aux Interfaces at the Université de Toulon et du Var; it consists of detecting the closed contours of the whitecap areas in an image (Massouh and Le Calve 1999). We believe the study of LP04 was the first to use a fully automated image processing method to calculate W from sea surface images.

It is the primary goal of this paper to describe the automated whitecap extraction (AWE) technique developed at the National University of Ireland, Galway. The development of the image processing technique to identify whitecaps was motivated by the need to analyze large numbers of sea surface images in a fast and objective manner. Callaghan et al. (2008, hereafter CDS08) provide a very brief overview of the processing principle of AWE, but here we describe in more detail the image processing algorithm. AWE was used to process the images analyzed in Callaghan et al. (2007) and an early version of AWE was used in Callaghan and White (2006). Section 2 provides a brief review of some methods of W determination from previous studies. Section 3 documents AWE, and some results and the discussion are presented in section 4. We present our conclusions in section 5.

2. Previous digital image analysis techniques

Thresholding is a commonly used digital image analysis technique to separate objects within digital images based on their intensity values. Typically, whitecaps are brighter than the background water surface and therefore have a greater intensity value. Manual thresholding allows a human analyst to identify a suitable pixel intensity value that is used to separate whitecaps from unbroken background water. All the pixels in an image with intensity values greater than this threshold value are assumed to be whitecaps and are assigned the maximum possible intensity value. All the other pixels with intensity values equal to or less than the threshold value are assigned the minimum possible intensity value. This produces a black and white image in which any identified whitecaps can be easily seen. Using this basic principle, many authors have analyzed sea surface images for W (e.g., Nordberg et al. 1971; Ross and Cardone 1974; Monahan et al. 1984; Asher and Wanninkhof 1998; Xu et al. 2000; Asher et al. 2002; Stramska and Petelski 2003).

Thresholding has also been employed to analyze batches of sea surface images (e.g., Kraan et al. 1996 and Sugihara et al. 2007, hereafter ST07). Using this approach, a single threshold is applied to all the images taken within a certain sampling period and an average value of W is obtained from all images for that period. This process is repeated for a number of thresholds and one final suitable threshold is then chosen. The choice is made so that the value of W does not vary much with changes in the threshold.

Both individual image analysis and batch image analysis have advantages and disadvantages. Typically, threshold choice is dictated by a number of factors, including both environmental and experimental conditions. The ambient illumination in which an image was taken affects the threshold choice because it impacts the overall brightness of the image. Ambient illumination can change on the order of seconds; thus, two images separated by only a few seconds often require different thresholds (e.g., Stramska and Petelski 2003; Asher et al. 2002; Asher and Wanninkhof 1998). This environmental effect is more severe for days with partial nonstationary cloud cover but less severe for overcast days with uniform cloud cover. Variable camera inclination angles also affect threshold choice. For example, cameras are often fixed to the bow of a research vessel, and the unstable nature of this platform impacts the overall brightness of the sea surface images because the image footprint can be a variable distance from the horizon. Individual image analysis allows a human analyst to adjust the appropriate threshold to reflect possible environmental and experimental impacts on image brightness and hence threshold choice. Typically, however, the manual setting of thresholds for individual image analysis is a very time-consuming procedure and it does not easily facilitate the analysis of large numbers of images. Given the intermittent and nonuniform nature of wave breaking, it is advantageous to analyze a large dataset of images for each W value. CDS08 suggest that for a 20-min sampling interval, hundreds of images are needed to yield convergent values of W.

The use of batch image analysis more easily facilitates the analysis of large numbers of images per individual

W value. Using this approach, ST07 analyzed 600 images per W data point. Batch image analysis assumes the suitability of a single threshold for each single batch of images and does not provide the flexibility to account for changing ambient illumination and platform instability. Therefore, the use of batch image analysis is probably more suited to sets of images collected from a stable platform in overcast conditions.

3. AWE method

a. Method overview

The AWE technique is a robust, automated, and objective method of identifying whitecaps in sea surface images that uses thresholding as a means to separate whitecaps from unbroken background water. AWE strives to combine the best features of individual and batch image analysis. AWE inspects each individual image and uniquely determines an appropriate threshold to separate whitecaps from background water. This feature has the advantage that the threshold is unique to each processed image and reflects the ambient illumination in which the image was taken. The threshold determination, based on derivative analysis, is automated and does not require input from a human analyst. This feature allows large numbers of images to be analyzed in a relatively short period of time in an objective manner. AWE has been developed using several image datasets collected from a wide range of platforms (e.g., ferry boat, research vessel, lighthouse, and tower), using different camera inclination angles and azimuth angles and using images that were taken in a wide range of environmental conditions.

The images we have used to illustrate the mechanics of AWE were taken during the Marine Aerosol Production (MAP) cruise aboard the Research Vessel (R/V) *Celtic Explorer* in June 2006 in the northeast Atlantic Ocean. MAP is an international multi-institute campaign whose main goals are to investigate the production and composition of the marine aerosol. The images were taken using a digital video system mounted ~19 m above sea level at a frequency of 0.5 Hz. The images had an initial pixel resolution of 576 × 768 but were cropped because of inconsistent image borders. After cropping, the images had pixel dimensions of 535 × 715. The camera had an inclination angle of approximately 84° from the nadir and the camera lens focal length was 50 mm. The image footprint area was calculated to be ~4997m^2.

b. Mechanics of AWE

AWE begins by reading in an RGB image and converting it into a grayscale intensity image of double precision. In the intensity image, all pixels have a value in a range between 0 (black) and 1 (white). AWE employs a thresholding technique to distinguish between whitecaps and background water. Initially, it is assumed that all intensity values above a predefined minimum value are potentially suitable thresholds. AWE applies these multiple potential thresholds to each image. These potential thresholds range in value from an intensity value close to the maximum intensity value of the image to a predefined minimum intensity value. The difference in intensity value between each pair of contiguous potential thresholds is 0.01. For each potential threshold, the number of pixels with intensity values greater than the threshold value is calculated. Using these numbers of pixels and starting at the highest intensity value, the percentage increase in number of pixels detected between contiguous pairs of thresholds (hereafter PIP) is calculated and is given by

$$\mathrm{PIP}(i) = \frac{P(i) - P(i + 0.01)}{P(i)} \times 100, \qquad (1)$$

where $P(i)$ represents the number of pixels with intensity values greater than an intensity value of i. The variable i ranges in value between the user-defined maximum and minimum intensity value; $P(i)$increases as the threshold intensity i decreases. Following this procedure, AWE produces a plot such as the one shown in Fig. 1. It is termed the image structure in further discussions and is central to the image processing technique.

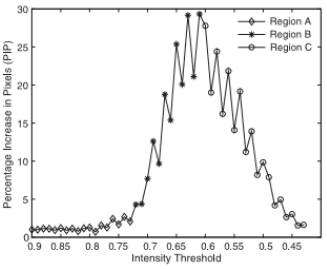

FIG. 1. The variation of PIP with intensity threshold for a sea surface image of a whitecap. This is termed the image structure. Each symbol corresponds to a different region within the image structure that enables AWE to determine the appropriate threshold to separate whitecaps from background water.

1. Read RGB, grayscale of black (0) and white (1)
2. Initial assumption:
   a. All intensity values above a minimum could be thresholds
   b. Applies each threshold to each image
   c. For each threshold, number of pixels above threshold are calculated
   d. Start as highest threshold value, PIP calculated: % increase in pixels is calculated between contiguous pairs of thresholds
3. $$\mathrm{PIP}(i) = \frac{P(i) - P(i + 0.01)}{P(i)} \times 100,$$

FIGURE 1

c. Image structure

The image structure shows how the PIP varies as the threshold decreases. The PIPs for threshold values within approximately 0.05 of the maximum intensity value of the image are typically very noisy and are omitted from the image structure for clarity. Figure 1 displays a typical image structure for a sea surface image with a whitecap present. It will be used as an example to help identify the various regions within the image structure used in derivative analysis and to describe the image structure in more detail. The absolute values that delimit each of the three regions are particular to this illustrative example and typically vary for different images.

For the purposes of description, the image structure is divided into three regions: region A, region B, and region C. Each of these three regions corresponds to distinct structures within the original image and they are used in the threshold determination process. The image structure is the key piece of information that is needed to determine the threshold for each image; it is also used to recognize when an image does not contain any whitecaps. The image structure will differ for different images. It reflects the various features within an image and also the ambient illumination in which the image was taken. The entire image structure can be shifted toward higher or lower intensity values, depending on both the ambient illumination and the features within an image. As a result, it is the shape of the image structure, rather than its absolute value, that is important in the threshold determination process. This is a key feature of AWE that ensures that the determined threshold reflects changes in ambient illumination.

Beginning at the intensity threshold value of 0.90 shown in Fig. 1, the PIP at each new threshold remains relatively constant until the threshold value of 0.73. This section of the image structure is termed region A in the following discussion. Between the threshold value of 0.72 and the threshold value of 0.61, there is an average steady increase in the PIP for each new lower threshold; this section of the image structure is termed region B. Between the threshold value of 0.60 and the lowest threshold value, the PIP decreases steadily for each new lower threshold; this section of the image structure is termed region C.

Region A corresponds to all the thresholds that uniquely identify the different intensity levels within the spatial structure of a whitecap. A typical spatial intensity structure of a whitecap reveals that the pixels at the center of the whitecap have the largest intensities. The pixel intensity values decrease with increasing proximity to the whitecap edge because the whitecap naturally thins out with the decrease in bubble concentration; therefore, the thresholds at the upper end of region A represent the central part of the whitecap. As the threshold is iteratively lowered, more and more of the whitecap is detected until the pixels at the edge of the whitecap are detected. The PIP at each new lower threshold can vary from image to image but is typically relatively constant within region A. This imparts a very characteristic shape to region A in comparison with regions B and C.

The transition between regions A and B represents a change in the type of pixels that are detected as the threshold is lowered. The first intensity threshold of region B represents the point at which both whitecap pixels and background water pixels are detected. At each new lower threshold, more and more of the unbroken background water pixels are detected, along with the higher-intensity whitecap pixels. Region B is easily recognized because of a relatively sharp and steady increase in PIP values with decreasing intensity threshold.

Finally, region C is characterized by steadily decreasing PIP values for each new lower threshold. This can be explained by the fact that as the threshold approaches the lower intensity values of the image, the vast majority of the pixels have already been detected.

The identification of regions A, B, and C is possible under conditions of extreme whitecap coverage. We investigated this using several images containing whitecaps that were iteratively cropped to remove part of the background water from the image. At each iteration, the percentage whitecap coverage of the image increased. The procedure was continued until approximately 60% of the images consisted of whitecaps. Regions A, B, and C were clearly identifiable in the image structure of the test images.

d. AWE threshold determination

The transition between regions A and B in the image structure represents the intensity value that should be chosen to discriminate between whitecap and background water. This intensity threshold is chosen using derivative analysis. Typically the first, second, and third derivatives of the image structure are needed to identify the transition between regions A and B. Because of the erratic nature of the image structure as seen in Fig. 1, it is smoothed twice using a four-point running mean before calculating its first derivative. The derivatives are calculated as follows:

$$\frac{d[\phi(i)]}{di} = \frac{\phi(i) - \phi(i + 0.01)}{\Delta i}, \qquad (2)$$

Image structure
- How PIP varies as threshold increases
- Fig 1 as an example
- Values that delimit image regions depend on each image. How are they decided?
- Regions in image correspond to different structures
- Image structure reflets things like ambient illumination
- Shape in image structure important in threshold determination

See fig 1
- Region A: Whitecap
- Region B: whitecap and water
- Region C: decrease in pixeel % as most pixels have been detected

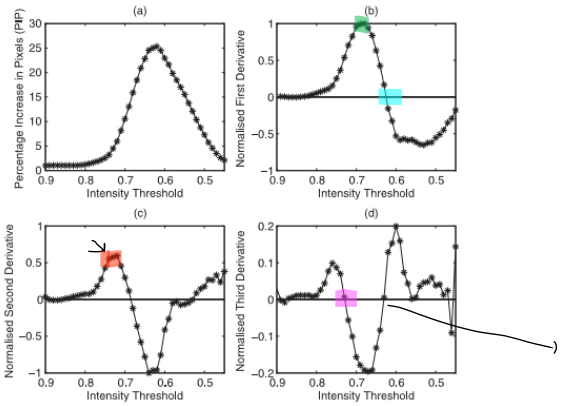

FIG. 2. (a) Smoothed image structure depicted in Fig. 1. (b)–(d) Normalized smoothed (b) first, (c) second, and (d) third derivative of (a).

where i is the intensity value, $\Delta i = 0.01$, and ϕ can represent the PIP and its first and second derivatives. After the first derivative of the image structure has been calculated, it is smoothed once using the four-point running mean and is subsequently used to calculate the second derivative. Similarly, the second derivative is smoothed and used to calculate the third derivative. The smoothed image structure and smoothed first, second, and third derivatives of the image structure depicted in Fig. 1 are shown in Fig. 2. The smoothing is necessary to facilitate easier and more accurate automated detection of the regions within the image structure. The intensity level at which the maximum local PIP second derivative occurs, as depicted in Fig. 2c, marks the first point in region B of the image structure. This point represents the first detection of background water pixels as well as all the whitecap pixels. Therefore, it is the next highest intensity level that represents the appropriate value to be chosen as the image threshold that separates whitecaps from the background water.

Starting at the lowest threshold intensity value and working toward higher intensity values, AWE locates the position of the first negative to positive zero crossing of the first derivative. This identifies the transition from region C to region B. This occurs at a threshold value of between 0.62 and 0.63 in Fig. 2b and it is used as a lower threshold limit from which to proceed with the rest of the operations of AWE.

In Fig. 2b, the first derivative reaches a local maximum value at an intensity value of 0.68. This corresponds to the location of the largest increase in detected pixels between pairs of threshold values within region B. This is a characteristic feature of region B of the image structure; it typically occurs approximately midway through region B. AWE uses the second derivative of the image structure to locate this maximum value of the first derivative that is found at the second derivative zero crossing above the transition between regions C and B.

It can be seen from Fig. 2c that the second derivative of the image structure reaches a positive local maximum value at a threshold intensity of 0.72. It is this intensity value that marks the position of the first intensity threshold value within region B. Therefore, the value 0.73 is determined to be the most appropriate threshold to separate whitecaps from background water; it is located using the third derivative as shown in Fig. 2d. The closest intensity threshold to the zero crossing is chosen as the final threshold for the image. Figure 3 shows the original image and a binary image that is the result of

AWE threshold determination
- Transition between A and B: intensity value that should be used as threshold
- 1st 2nd and 3rd derivatives needed to identify transition. Why 3?
- Also needs smoothing bc too noisy

Lower threshold?

FIG. 3. (a) An example of an original whitecap image; (b) the subsequent AWE processed binary image. The result of the AWE image processing technique shows the detected whitecap in white and the background water in black.

applying the threshold chosen by AWE. The ratio of white pixels to black pixels is converted into a percentage value, which is the W value for this image. Repeating this process, AWE can analyze large numbers of images in a fast and repeatable manner.

e. Non-whitecap images

Equally as important as identifying whitecaps in an image is the ability to recognize when an image contains no whitecaps. This is especially important at wind speeds below about 7 m s^{-1} when the frequency of wave breaking is greatly reduced and an image dataset may contain large numbers of images without any whitecaps present. Using manual individual image analysis methods it is straightforward for a human analyst to recognize when an image does not contain any whitecaps. However, when using an automated image analysis technique, it is vital that spurious values of W values are not produced for images that do not contain any whitecaps. AWE determines whether or not an image contains whitecaps using the image structure. Figure 4 shows the smoothed image structure and its first derivative from an image with no whitecaps present. The image structure is markedly different from that in Fig. 1 and reveals its own characteristic shape. There is a steady decrease in the PIP at each lower threshold, which is reflected in the entirely negative first derivative. It is this specific characteristic property of the image structure's first derivative that enables AWE to recognize the absence of whitecaps in an image.

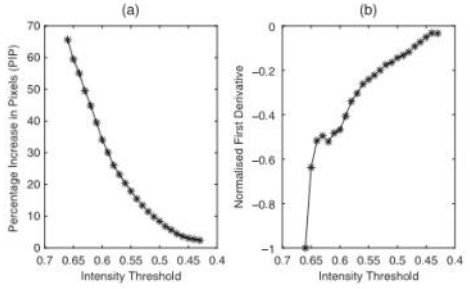

FIG. 4. (a) The image structure of an image that does not contain any whitecaps. (b) The variation of the normalized smoothed first derivative of the image structure with intensity threshold.

Non whitecap images
- Winds below 7 ms
- Steady decrease in PIP: entirely negative first derivative - no whitecaps

TABLE 1. The table displays the percentage difference in W from the reference value for different thresholds. Each group consisted of 100 images and each group of images was taken at a different wind speed.

Threshold change	Group 1 (6.75 m s^{-1})	Group 2 (8.18 m s^{-1})	Group 3 (9.68 m s^{-1})	Group 4 (12.05 m s^{-1})	Group 5 (13.52 m s^{-1})	Group 6 (16.43 m s^{-1})	Group 7 (18.11 m s^{-1})
+0.04	−32	−33	−28	−31	−29	−32	−33
+0.03	−26	−27	−23	−25	−23	−25	−27
+0.02	−19	−20	−17	−19	−18	−19	−20
+0.01	−10	−10	−9	−9	−9	−9	−10
0	0	0	0	0	0	0	0
−0.01	23	20	19	19	17	18	20
−0.02	62	42	42	37	34	35	40
−0.03	163	82	94	72	67	69	83
−0.04	371	135	162	112	105	108	134

f. Threshold evaluation, sensitivity, and uncertainty in W

1) THRESHOLD EVALUATION AND SENSITIVITY

Threshold choice is critical when analyzing sea surface images for W. In manual image analysis, the precise threshold that separates whitecaps from unbroken background water can often be difficult for a human analyst to determine. Stramska and Petelski (2003) processed each individual image using two thresholds that differed in intensity value by 0.01 because of the difficulty in deciding the most suitable threshold. They chose two threshold values such that the W value for each image did not vary much between each threshold; the final W value was the average of these two values. We have also experienced this difficulty when manually determining image thresholds. It is therefore difficult to obtain objective estimates of whitecap coverage for individual images with which to evaluate the accuracy of AWE. However, to evaluate the AWE threshold choice and the subsequent sensitivity of threshold choice, we examined how values of W changed as the AWE-derived threshold was increased and decreased.

To evaluate the threshold choice and sensitivity using AWE, we took seven groups of 100 images that had been analyzed using AWE and modified the individual image thresholds to investigate how W changed with changing threshold. To do this, each image in a group was reprocessed with a different threshold value to the original AWE-derived threshold. Thresholds were modified in increments of 0.01 from −0.04 to +0.04 of the original threshold; W was then recalculated for all 100 images in each group and averaged to yield eight new W values for each of the seven groups of images. The original AWE-derived W average values were then used as reference values against which the new values were compared. The percentage differences (PDs) between the reference W values and those using the modified thresholds are displayed in Table 1 in columns 2 to 7. Below each group number is the wind speed at which the images in that group were taken. Column 1 displays the magnitude of the threshold modification. The fifth row from bottom represents the reference W values for each group as computed using AWE.

Taking group 4 in Table 1 as an example, the change in percentage difference values with decreasing threshold remains relatively constant up until the reference threshold (i.e., in the range of threshold change from +0.04 to 0). Within this range of threshold values, any contiguous pair results in similar values of W. The method of threshold choice implemented by Stramska and Petelski (2003) would be analogous to choosing the final pair of contiguous threshold values in this range. When the threshold value is decreased to values below the AWE-derived threshold, the percentage differences increase. Employing the logic developed in section 3d, at the transition in intensity value between whitecaps and background water there should be a relatively large increase in the number of pixels detected with decreasing threshold. From Table 1, the change in percentage difference values doubles when the threshold is changed by −0.01, remains relatively unchanged at −0.02, and approximately doubles again at −0.03. Therefore, to achieve complete detection of whitecap pixels without detection of background water, the last threshold displaying a relatively constant change in percentage difference is the most appropriate, and it is this threshold that is chosen for each image using AWE.

An inspection of the percentage difference values in Table 1 indicates that as the threshold decreases below the AWE-determined threshold, the relative number of pixels detected increases. This shows that underestimating the threshold for an image would result in a larger deviation from the true W value for that image than overestimating it would. The threshold choice of AWE presented has a resolution intensity value of 0.01, which leads to a measurement error of ±0.01. This information can subsequently be used to determine the

Threshold evaluation
- How W changes as AWE threshold changes
- Sensitivity:
  - 7 groups of 100 images with calculated thresholds -change them-recalculate W
  - Percentage change with increasing threshold relationshp -cte
  - Negative changes: more drastic changes
  - Better to overestimate than underestimate. Derived measurement error 0.01

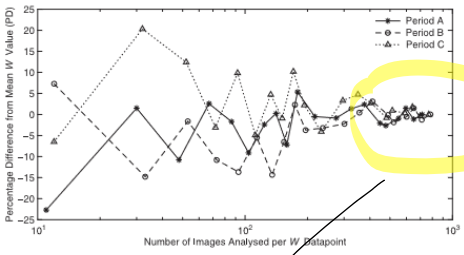

FIG. 5. The variation in the percentage difference for three separate measurement periods with increasing numbers of images analyzed per *W* data point. The PD oscillates and begins to decrease with an increase in the number of images analyzed per *W* data point. The PD is a measure of the uncertainty of the *W* data point.

measurement error associated with each individual *W* data point. Assuming that the AWE-chosen threshold is correct, an overestimation of the threshold by a value of 0.01 would lead to a *W* value within approximately 10% of the true value, whereas an underestimation of the threshold would give a *W* value within approximately 20% of the true value (based on the information given in Table 1).

2) UNCERTAINTY IN *W* VALUES

Often whitecap studies relating *W* values to wind speed have been characterized by a large degree of scatter. Because *W* depends not only on wind speed but also on other parameters such as sea state, part of this data scatter is likely due to an underrepresentation of all the relevant parameters that affect *W*. However, at least some of the data scatter may also be due to processing an inadequate number of images with which to calculate each *W* data point. Reducing the scatter of *W* datasets enables a more accurate characterization of the influence that physical and environmental variables have on *W*. The automated feature of AWE enables large numbers of images to be analyzed to calculate each individual *W* data point and hence helps to reduce the uncertainty in *W* measurements arising from undersampling.

To demonstrate the decrease in *W* uncertainty when using a large number of images to calculate *W*, we use *W* results obtained from three separate half-hour sampling periods during the MAP campaign (in a manner similar to CDS08). The value of *W* was recalculated using 20 subsamples of the total number of images collected during each period. The total number of images analyzed for each of these three periods was 715, 782, and 769, respectively. Each subsample corresponded to selecting images at different intervals from the total number of images. The largest subsample simply yielded the maximum number of images within each period. The smallest subsample corresponded to a subsample of approximately 10 images sampled at regular intervals. The mean *W* value for each subsample was then calculated. The reference mean *W* value used corresponded to the mean of all the images in a certain period. This was the same as the mean *W* value of the largest subsample. The percentage difference from the reference mean of each of the 20 *W* values was calculated for all of the three periods (periods A, B, and C); it is an indication of the uncertainty of the *W* measurement. The results are plotted in Fig. 5. The figure demonstrates the increasing convergence of *W* and consequent decrease in *W* uncertainty, with increasing numbers of images analyzed. The PD oscillates initially before converging to a value of approximately ±5% of the reference mean *W* for a subsample size of 200 images. The PD further decreases to ±3% for a subsample size of approximately 500 images.

These results are similar to those of CDS08, who used images obtained in very different experimental conditions. Images used in that study were taken from a stable platform located in a coastal zone. They noted that the PD decreased to ±4% when using a subsample of 300 images from a total image set of 1200 collected in a 20-min sampling period. The camera height, incidence angle, and lens focal length were different between the two field campaigns, which resulted in different viewing areas for each image set. Whitecap datasets have been

Uncertainty in W values
-

TABLE 2. A comparison of W values predicted by the wind speed–only models from previous studies at discrete wind speeds.

Previous study	4 m s^{-1}	6 m s^{-1}	8 m s^{-1}	10 m s^{-1}	12 m s^{-1}	14 m s^{-1}
CDS08	0.011	0.055	0.172	0.415	0.853	1.569
ST07	0.006	0.051	0.173	0.41	0.802	1.386
LP07	0.024	0.104	0.299	0.674	1.312	2.303
LP04	0.018	0.085	0.259	0.614	1.247	2.267

typically characterized by a large degree of scatter, and many previous whitecap studies have used tens of images or less to calculate individual W data points. However, from Fig. 5 in this study and from Fig. 2 in CDS08 it is clear that hundreds of images are needed to reduce the uncertainty and achieve convergent W data points.

4. Results and discussion

AWE has been successfully implemented in the coastal zone study of CDS08. To evaluate the absolute values of W as computed using AWE, we now compare the wind speed–only models of W from CDS08 [their Eq. (1)] to similar whitecap models developed in the coastal zones studies of ST07 (from their Fig. 9), LP04 [their Eq. (9)], and LP07 [their Eq. (8)]. All models are evaluated at wind speeds of 4, 6, 8, 10, 12, and 14 m s^{-1}. Calculated W values from all models are given in Table 2.

The W values predicted by the CDS08 relationship lie between the values predicted by the other studies. This indicates that AWE produces W results that are comparable to those of other studies in similar environments that use different image analysis techniques.

The key to the successful implementation of AWE is the quality of the sea surface images to be analyzed. Images with constant background water illumination throughout the image, good contrast between whitecaps and background water, and images free from contamination produce a well-defined image structure. Before implementation of AWE, it is critical that all contaminated images are removed from the image dataset. Two common forms of image contamination are uneven image illumination and sun glint. Uneven image illumination due to sky reflection, partial blocking of incident radiation by clouds, or raindrops on the camera lens can adversely affect the success of whitecap identification. This can preclude the use of a single threshold to accurately determine W from sea surface images without first cropping the image. Unevenly illuminated images often contain bright areas of background water that have intensity values comparable to the intensity values of whitecaps, thus making the whitecaps indistinguishable from the background water in an image. Also, the strong presence of sky reflection in an image that does not contain any whitecaps can produce an image structure that is similar in shape to an image that actually contains a whitecap. As a result, image contamination from sky reflection can lead to the incorrect analysis of images that contain whitecaps and can also lead to the analysis of images that do not contain whitecaps. The presence of sun glint in an image also renders the image unsuitable for analysis. Sun glint is sun light that has been specularly reflected from the sea surface. It is characterized by high intensity values and it is indistinguishable from whitecaps. When sea surface images are taken from aircraft, the presence of clouds that lie between the sea surface and the camera can be a source of image contamination. These images must either be cropped to remove the cloud object or discarded completely before implementation of AWE.

Many studies have reported that images had to be discarded or cropped to remove the contaminating effects of sun glint and sky reflection (e.g., CDS08; ST07; Asher et al. 2002; Kraan et al. 1996). The probability of image contamination from sun glint and sky reflection can be reduced by careful positioning of the camera at a suitable azimuth angle from the sun. Experimental campaigns do not always offer the possibility for ideal camera positioning, and it can often be difficult to achieve images of suitable quality for automated analysis. For example, camera position is commonly set in a fixed position at the beginning of a research cruise; consequently, the ship's heading controls the orientation of the camera. However, where possible the camera position should be optimally placed to reduce image contamination. With an azimuth angle of 0°, image contamination can be at its most severe. As the azimuth angle approaches 180°, the contamination effects typically diminish. To the best of our knowledge, no studies have been conducted to evaluate the optimum azimuth angle for camera position in whitecap studies; however, through experience we have found the minimum azimuth angle needed to eliminate sun glint is approximately 60°. Ideally, a minimum azimuth angle of 90° should be maintained. If the position of the camera is fixed, this can be achieved by setting a poleward-facing camera position. It must be noted, however, that using a fixed azimuth angle does not always guarantee the total elimination of sun glint or sky reflection contamination because other factors that can lead to sun glint and sky reflection contamination include the elevation of the sun in the sky and the wave field slope.

Typically, the image structure for each analyzed image results in an erratic sawtooth appearance, such as the image structure depicted in Fig. 1. To facilitate less

Results and discussion

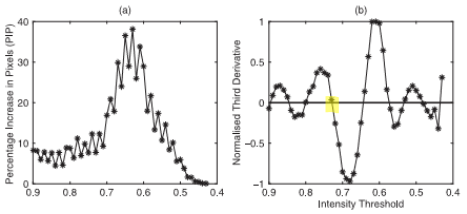

FIG. 6. (a). Image structure of a sea surface image with a whitecap. (b) Smoothed normalized third derivative of (a). The figure illustrates how sometimes the AWE-derived threshold is too high and does not correspond to the optimum threshold. In this scenario, AWE performs two checks to ensure the optimum threshold is chosen.

complicated processing, the image structure and subsequent derivatives are smoothed. However, because of this smoothing, sometimes the threshold determined by AWE may not occur exactly at the transition between regions A and B in an image structure. Figure 6 shows the image structure and the smoothed third derivative of an image containing a whitecap. As can be seen from the image structure, region A finishes at a threshold value of 0.71 and region B begins at a threshold value of 0.70. Therefore, the most appropriate threshold for this image is 0.71. However, from the plot of the third derivative, AWE would choose a slightly higher value of 0.73 as the threshold for the image. To ensure that the correct threshold is chosen, AWE performs two simple checks using the unsmoothed image structure to ensure that the chosen threshold for each image is as close as possible to the transition between regions A and B of the image structure. As can be seen from Fig. 6b, the PIPs at threshold values of 0.73 and 0.71 are closer in value to each other than to the PIP at a threshold of 0.72. Using this information, AWE chooses the lower threshold value of 0.71 as the final threshold for the image. On occasion, also because of smoothing, AWE chooses the penultimate threshold value within region A of the image structure. Using Fig. 6b as an example, this would correspond to a threshold value of 0.72. When this occurs, the threshold is simply lowered by a value of 0.01 if the PIP at the lower threshold is less than the PIP at the originally chosen threshold. Again using Fig. 6b as an example, this would mean lowering the threshold from 0.72 to 0.71.

Using the nomenclature of Monahan and Lu (1990), whitecaps can be broadly separated into two groups. Stage A whitecaps are those that are formed at the crests of actively breaking waves. The whitecap depicted in Fig. 3 is an example of a stage A whitecap. The wave crest is breaking toward the camera. Stage B whitecaps refers to the more diffuse foam that is present on the sea surface after a wave has finished breaking. The patch of foam in Fig. 7a is an example of a stage B whitecap. Figures 7b–d depict the processed image, the image structure, and the third derivative of the image structure, respectively. Stage B whitecaps consist of the decaying foam patch of stage A whitecaps; they typically have longer lifetimes than stage A whitecaps. The intensity level of a stage A whitecap and that of a young stage B whitecap are relatively similar, so the intensity cannot be used as a single criterion with which to distinguish between the two stages of whitecaps (Stramska and Petelski 2003). As a result, the quantity measured by AWE represents the total whitecap coverage from both stage A and stage B whitecaps.

5. Conclusions

We have presented an automated whitecap extraction (AWE) image processing technique for the identification of whitecaps in sea surface images. Whitecap datasets are typically characterized by a large degree of scatter and many whitecap models exist in the literature (see Anguelova and Webster 2006). At least part of this data scatter may be due to the analysis of insufficient numbers of images, which results in nonconvergent values of W. Similarly to the study of CDS08, we have shown that increasing the number of images with which to calculate W results in more convergent values of W, which reduces the uncertainty associated with each W data point and can help reduce some of the characteristic data scatter. AWE facilitates the analysis of sea surface images without the need for a human analyst,

Some checks to make sure correct threshold is chosen

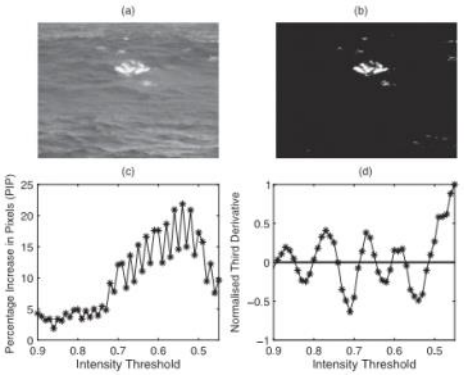

FIG. 7. (a) Original image showing a stage B whitecap. (b) Processed binary image showing the detected whitecap. (c) Image structure. (d) Normalized smoothed third derivative of (c).

which enables the possibility of analyzing large numbers of images to produce values of W.

AWE uses thresholding to separate whitecaps from background water. For individual sea surface images, AWE uniquely determines the appropriate threshold with which to separate whitecaps from background water. To achieve this, a distinct image structure is calculated for each image and is then used to find the appropriate threshold. The image structure is a function of the features within an image and also of the ambient illumination in which the image was taken. Distinct differences in the shape of the image structures of images with and without whitecaps enable AWE to determine whether an image contains a whitecap or not. Changing ambient illumination leads to differences in the absolute values of the image structure but does not affect its pattern. Therefore, the threshold determined for each image reflects the ambient illumination in which the image was taken. This is an important feature of AWE because changing ambient illumination can lead to markedly different thresholds for images taken only seconds apart.

AWE employs derivative analysis to determine the appropriate threshold for each image. AWE determines the correct threshold value by using information from the first, second, and third derivatives of the image structure. The chosen threshold represents the lowest intensity value within an image that detects only the whitecap pixels and not the background water. The use of derivative analysis ensures an objective choice of threshold for each image and requires no input from a human analyst.

The success of AWE is dependent on the quality of the sea surface images collected. Often whitecap image datasets require screening by a human analyst to identify all unsuitable images that need to be cropped before analysis to remove the contaminated regions of the image or discarded completely. Images contaminated by sun glint and uneven illumination cannot be successfully analyzed. Raindrops on the camera lens degrade image quality and render them useless for analysis. In the case of images taken from aircraft, all images contaminated by clouds should be removed. Where possible, the careful positioning of the camera can help to avoid contamination from the effects of sun glint and uneven illumination caused by sky reflection. This can often be achieved by setting the camera in a poleward viewing position or maintaining a suitable camera azimuth angle of between approximately 60° and 180°.

Acknowledgments. The authors wish to thank Prof. C. O'Dowd (National University of Ireland, Galway) and Dr. G. de Leeuw (Finnish Meteorological Institute) for

permission to use images from the Marine Aerosol Production (MAP) campaign and L. H. Cohen (TNO Security and Defense, The Hague, Netherlands) for his efforts recording the images. The lead author acknowledges financial support through the EU INTERREG IIIA (Ireland–Wales) Programme, administered by the Welsh European Funding Office (WEFO). We acknowledge J. Kleiss for providing the image footprint area. We acknowledge the valuable comments of L. Valentini on an early draft of the manuscript and the helpful comments of two reviewers.

REFERENCES

Anguelova, M. D., and F. Webster, 2006: Whitecap coverage from satellite measurements: A first step towards modeling the variability of oceanic whitecaps. *J. Geophys. Res.*, **111,** C03017, doi:10.1029/2005JC003158.

Asher, W. E., and R. Wanninkhof, 1998: The effect of bubble-mediated gas transfer on purposeful dual-gaseous tracer experiments. *J. Geophys. Res.*, **103** (C5), 10 555–10 560.

——, L. M. Karle, B. J. Higgins, P. J. Farley, I. S. Leifer, and E. C. Monahan, 1996: The influence of bubble plumes on air–seawater gas transfer velocities. *J. Geophys. Res.*, **101,** 12 027–12 041.

——, J. Edson, W. McGillis, R. Wanninkhof, D. T. Ho, and T. Litchendorf, 2002: Fractional area whitecap coverage and air–sea gas transfer velocities measured during GasEx-98. *Gas Transfer at Water Surfaces, Geophys. Monogr.*, Vol. 127, Amer. Geophys. Union, 199–203.

Callaghan, A. H., and M. White, 2006: Observations of the effect of fetch on whitecap coverage in the Irish Sea. *Proc. SOLAS Ireland Workshop 2006*, Galway, Ireland, Environmental Change Institute, 70–75.

——, G. de Leeuw, and L. H. Cohen, 2007: Observations of oceanic whitecap coverage in the North Atlantic during gale force winds. *Proc. 17th Int. Conf. on Nucleation and Atmospheric Aerosols*, Galway, Ireland, Committee on Nucleation and Atmospheric Aerosols, 1088–1092.

——, G. B. Deane, and M. D. Stokes, 2008: Observed physical and environmental causes of scatter in whitecap coverage values in a fetch-limited coastal zone. *J. Geophys. Res.*, **113,** C05022, doi:10.1029/2007JC004453.

Frouin, R., S. F. Iacobellis, and P.-Y. Deschamps, 2001: Influence of oceanic whitecaps on the global radiation budget. *Geophys. Res. Lett.*, **28,** 1523–1526.

Gordon, H. R., 1997: Atmospheric correction of ocean color imagery in the Earth Observing System Era. *J. Geophys. Res.*, **102** (D14), 17 081–17 106.

Guan, C., W. Hu, J. Sun, and R. Li, 2007: The whitecap coverage model from breaking dissipation parameterizations of wind waves. *J. Geophys. Res.*, **112,** C05031, doi:10.1029/2006JC003714.

Kraan, C., W. A. Oost, and P. A. E. M. Janssen, 1996: Wave energy dissipation by whitecaps. *J. Atmos. Oceanic Technol.*, **13,** 262–267.

Lafon, C., J. Piazzola, P. Forget, O. Le Calve, and S. Despiau, 2004: Analysis of the variations of the whitecap fraction as measured in a coastal zone. *Bound.-Layer Meteor.*, **111,** 339–360.

——, ——, ——, and S. Despiau, 2007: Whitecap coverage in coastal environment for steady and unsteady wave field conditions. *J. Mar. Sys.*, **66,** 38–46.

Lewis, E. R., and S. E. Schwartz, 2004: *Sea Salt Aerosol Production: Mechanisms, Methods, Measurements, and Models—A Critical Review*. *Geophys. Monogr.*, Vol. 152, Amer. Geophys. Union, 413 pp.

Massouh, L., and O. LeCalve, 1999: Measurements of whitecap coverage during F.E.T.C.H. 98 experiment. *J. Aerosol Sci.*, **30,** (Suppl. 1), 177–178.

Monahan, E. C., and M. Lu, 1990: Acoustically relevant bubble assemblages and their dependence on meteorological parameters. *IEEE J. Oceanic Eng.*, **15,** 340–349.

——, P. Bowyer, D. Doyle, M. Higgins, and D. Woolf, 1984: Whitecaps and the marine atmosphere. University College Rep. 7, Galway, Ireland, 103 pp.

Nordberg, W., J. Conaway, D. B. Ross, and T. Wilheit, 1971: Measurements of microwave emission from a foam-covered wind-driven sea. *J. Atmos. Sci.*, **28,** 429–435.

O'Dowd, C. D., and G. de Leeuw, 2007: Marine aerosol production: A review of the current knowledge. *Philos. Trans. Roy. Soc.*, **365A,** 1753–1774.

Ross, D. B., and V. Cardone, 1974: Observations of oceanic whitecaps and their relation to remote measurements of surface wind speed. *J. Geophys. Res.*, **79,** 444–452.

Stramska, M., and T. Petelski, 2003: Observations of oceanic whitecaps in the north polar waters of the Atlantic. *J. Geophys. Res.*, **108,** 3086, doi:10.1029/2002JC001321.

Sugihara, Y., H. Tsumori, T. Ohga, H. Yoshioka, and S. Serizawa, 2007: Variation of whitecap coverage with wave-field conditions. *J. Mar. Sys.*, **66,** 47–60.

Wentz, F. J., 1992: Measurement of oceanic wind vector using satellite microwave radiometers. *IEEE Trans. Geosci. Remote Sens.*, **30,** 960–972.

Xu, D., X. Liu, and D. Yu, 2000: Probability of wave breaking and whitecap coverage in a fetch-limited sea. *J. Geophys. Res.*, **105** (C6), 14 253–14 259.